HIPPOCAMPUS 24:257–269 (2014)

Neuronal and Glial Alterations, Increased Anxiety, and Cognitive Impairment Before Hippocampal Amyloid Deposition in PDAPP Mice, Model of Alzheimer's Disease

Juan Beauquis,[1] Angeles Vinuesa,[1] Carlos Pomilio,[1] Patricio Pavía,[1] Verónica Galván,[2] and Flavia Saravia[1]*

ABSTRACT: In the context of Alzheimer's disease (AD), hippocampal alterations have been well described in advanced stages of the pathology, when amyloid deposition, inflammation and glial activation occur, but less attention has been directed to studying early brain and behavioral changes. Using an animal model of AD, the transgenic PDAPP-J20 mouse at 5 months of age, when no amyloid plaques are present and low cerebral levels of amyloid peptides are detectable, we found structural, morphological, and cellular alterations in the hippocampus. Young transgenic mice showed a reduced hippocampal volume with less number of pyramidal and granular neurons, which additionally exhibited cell atrophy. The neurogenic capability in this zone, measured as DCX+ cells, was strongly diminished and associated to alterations in cell maturity. A decrease in presynaptic synaptophysin optical density was detected in mossy fibers reaching CA3 subfield but not in Golgi stained- CA1 dendritic spine density. Employing confocal microscopy and accurate stereological tools we also found a reduction in the number of GFAP+ cells, along with decreased astrocyte complexity, suggesting a potential detriment of neural support. According with untimely neuroglial alterations, young PDAPP mice failed in the novel location recognition test, that depends on hippocampal function. Moreover, multivariate statistical analysis of the behavioral outcome in the open-field test evidenced an elevated anxiety score in Tg mice compared with age-matched control mice. In line with this, the transgenic group showed a higher number of c-Fos+ nuclei in central and basolateral amygdala, a result that supports the early involvement of the emotionality factor in AD pathology. Applying an integrative approach, this work focuses on early structural, morphological and functional changes and provides new and compelling evidence of behavioral alterations that precede manifest AD. © 2013 Wiley Periodicals, Inc.

KEY WORDS: PDAPP mouse model of Alzheimer's disease; pyramidal and granular neurons; DCX; glia; cognitive deficit and anxiety

INTRODUCTION

Progressive cognitive impairment, memory loss and personality changes are characteristic symptoms of Alzheimer's disease (AD), a neurodegenerative disorder associated with aging. Amyloid plaques, mainly composed of amyloid β (Aβ) peptide, and intracellular neurofibrillary tangles of aggregated hyperphosphorylated tau protein, constitute main histopathological hallmarks. Plaque load has been classically considered as the definitive feature to diagnose AD at autopsy (Blennow et al., 2006; Dubois et al., 2010). Loss of synapses and neurons, in addition to central inflammation, characterized by the presence of reactive glia around senile plaques, represent also important attributes associated to late stages of this disease in the brain from AD patients (Blennow et al., 2006). Most of the research done in animal models of AD evaluate brain changes in a context of full-blown amyloid pathology whereas less is known of the temporal dynamics of glial and neuronal changes at early stages of the disease, when therapeutic intervention seems more plausible. In a scenario characterized by the presence of Aβ soluble oligomers while amyloid deposits are not detectable, some alterations have been reported in AD models, suggesting a presynaptic failure, associated to initial stages of the disease (Palop and Mucke, 2009). Aβ oligomers can be more potent than Aβ fibrils and amyloid deposits in affecting synaptic integrity. Moreover, Aβ interferes in neuronal expression of synaptic activity-regulated genes (Palop et al., 2007). Synaptic dysfunction and altered glial support could lead to gradual decline in cognitive function, neuronal loss, and dementia as it was described in post mortem brain slices from AD patients (Albert, 2011). However, in AD models this is a controversial point where several authors have reported no changes in the number of neurons, specifically in mutated hAPP transgenic mice (Irizarry et al., 1997; Schaeffer et al., 2011), while few others detected CA1 pyramidal neuronal loss (Wright et al., 2013).

Reactive astrocytes, typically present on several neurodegenerative diseases including AD, lose many of their physiological homeostatic and supporting functions and contribute to neuronal dysfunction and cell

[1] **Instituto de Biología y Medicina Experimental CONICET and Departamento de Química Biológica, Facultad de Ciencias Exactas y Naturales, Universidad de Buenos Aires, Argentina;** [2] **Department of Physiology and The Barshop Institute for Longevity and Aging Studies, University of Texas Health Science Center at San Antonio, Texas**

Additional Supporting Information may be found in the online version of this article.

Grant sponsor: Alberto Roemmers Foundation; Grant sponsor: Agencia Nacional de Promoción de Ciencia y Tecnología of Argentina; Grant number: PICT 2011-#1012.

*Correspondence to: Flavia Saravia, Instituto de Biología y Medicina Experimental CONICET and Departamento de Química Biológica, Facultad de Ciencias Exactas y Naturales, Universidad de Buenos Aires, Obligado 2490 −1428- Buenos Aires, Argentina. E-mail: fesaravia@gmail.com

Accepted for publication 8 October 2013.
DOI 10.1002/hipo.22219
Published online 16 October 2013 in Wiley Online Library (wileyonlinelibrary.com).

death (Steele and Robinson, 2012). However, it is possible that more subtle non-classical astroglial changes could be present at earlier stages of the pathology. Recently, we described the presence of two astrocytic subpopulations in the hippocampus of PDAPP-J20 mice, a well-known model of AD, at a stage in which multiple amyloid plaques are found in the hippocampus. On the one hand, there are classical reactive astrocytes, showing enlarged soma and processes and found surrounding amyloid deposits, while, on the other hand, there are astrocytes located away from plaques, exhibiting nonclassical reactive changes in cell complexity and volume (Beauquis et al., 2013). In this line, Rodriguez et al proposed that, in various forms of dementia, glial atrophy and reactive astrogliosis may develop in parallel during the neurodegenerative process (Rodriguez et al., 2009).

As mentioned, one major concern in AD research is to find early brain alterations that precede fully-developed disease. In the present work we describe early astroglial, synaptic, and neuronal changes in the hippocampus of PDAPP transgenic mice, model of AD, at 5 months of age, when extremely low levels of brain beta amyloid peptides and minimal hippocampal amyloid deposition are detected. These anomalies, along with neuronal activation in central and basolateral amygdala, were associated with cognitive impairments and increased anxiety. Hence, we provide evidence of neuronal, glial, and behavioral alterations that are present before overt plaque deposition.

MATERIALS AND METHODS

Transgenic Mice

The derivation and characterization of PDAPP-J20 [hAPP(J20)] mice has been described elsewhere (Hsia et al., 1999; Mucke et al., 2000; Selkoe, 2000; Galvan et al., 2006; Roberson et al., 2007; Beauquis et al., 2013). This strain, a recognized model of AD, carries the hAPP gene with the familial AD Swedish and Indiana mutations, develops amyloid pathology and behavioral alterations in a progressive fashion (Galvan et al., 2006). and, also, shows evidence of Tau hyperphosphorylation (Simon et al., 2009). Transgenic mice were maintained by heterozygous crosses with C57BL/6J mice (Jackson Laboratories, Bar Harbor, ME) in our animal facility (Institute of Biology and Experimental Medicine, UBA–CONICET; NIH Assurance Certificate # A5072-01) and were housed under controlled conditions of temperature (22°C) and humidity (50%) with 12 h/12 h light/dark cycles (lights on at 7:00 am). PDAPP-J20 mice were heterozygous with respect to the transgene, verified by PCR using specific primers. All animal experiments followed the NIH Guide for the Care and Use of Laboratory Animals and were approved by the Ethical Committee of the Institute of Biology and Experimental Medicine. All efforts were done to reduce the number of mice used in the study as well as to minimize animal suffering and discomfort.

Determination of Aβ Levels

Human Aβ 1–40 and Aβ 1–42 peptides levels were measured in guanidine hemi-brain homogenates (n=7 mice per group) using specific sandwich ELISA assays (Invitrogen, USA) as previously described (Galvan et al., 2006; Spilman et al., 2010; Beauquis et al., 2013). The performance characteristics of the ELISA assays including precision, linearity of dilution, recovery, and antigenic specificity were determined and informed by the manufacturer. The minimum detectable amount of human Aβ1–40 was 6 pg/mL; while for Aβ1–42 was 13 pg/mL.

Tissue Processing

Animals were anesthetized with ketamine (80 mg/kg BW, i.p.; Holliday-Scott, Argentina) and xylazine (10 mg/kg BW, i.p.; Bayer, Argentina) and then transcardially perfused with 30 mL of 0.9% saline followed by 30 mL of 4% paraformaldehyde in 0.1 M phosphate buffer, pH 7.4. Brains were removed from the skull, dissected, fixed overnight in the 4% paraformaldehyde solution at 4°C and then cut coronally at 60 μm in a vibrating microtome (Vibratome 1000P). Sections were stored in a cryoprotectant solution (25% glycerol, 25% ethylene glycol, 50% phosphate buffer 0.1 M, pH 7.4) at −20°C until use. All immunohistochemical techniques and Congo red staining were performed on free-floating sections. For plaque load, cell number and morphometric analyses, six brain sections per mouse and five mice per experimental group were evaluated. In all detailed cases in the following sections, ventral and dorsal hippocampi were considered for plaque load, volume, cell counting, and optical density determinations.

Congo Red Staining and Amyloid Plaque Load

Amyloid plaque load was assessed in CA1 *strata radiatum* and *lacunosum-moleculare* from brain sections stained with Congo red (protocol available in Wilcock et al., 2006). Briefly, coronal brain sections were incubated for 5 min at room temperature (RT) in a solution containing 0.2% Congo red (Biopack, Argentina), 3% NaCl (to saturation) and 0.01% sodium hydroxide in 80% ethanol. After rinsing, sections were put on gelatin-coated slides, air-dried overnight, dehydrated using ethanol and cleared in xylene. Slides were coverslipped using Canada balsam (Biopack, Argentina). Images from Congo red stained sections were obtained under a 40X magnification in a Nikon Eclipse E200 microscope. Plaque load was determined as the percentage of the reference area that was occupied by Congo red-stained amyloid plaques. The reference area was measured by manually tracing *strata radiatum* and *lacunosum-moleculare* using Optimas software (Media Cybernetics). With the same software we determined Congo red stained area using an operator-determined gray value threshold. As a positive control we used brain sections from 20-month-old Tg mice that had multiple amyloid plaques in the hippocampus.

Immunohistochemistry

NeuN immunohistochemistry was done to estimate the volume of hippocampal regions and the corresponding density of

neurons in CA1, CA3, and dentate gyrus (DG) areas and also cell diameter estimation. Presynaptic densities were assessed through synaptophysin detection. Doublecortin (DCX) immunohistochemistry was done to evaluate neurogenic capability in the DG. Additionally, GFAP immunohistochemistry was done to determine number, volume, and morphology of hippocampal astrocytes. c-Fos immunohistochemistry was performed to assess neuronal activity in the amygdala and ventral hippocampus. After blocking of nonspecific antigenic sites, sections were incubated overnight at 4°C with the following primary antibodies: rabbit polyclonal anti-GFAP (1:300, G-9269, Sigma), mouse monoclonal anti-NeuN (1:250, MAB377, Chemicon, USA), goat polyclonal anti-DCX (1:400, SC-8066, Santa Cruz Biotechnology, USA), mouse monoclonal anti-synaptophysin (1:500, MAB5258, Chemicon, USA) or rabbit polyclonal anti-c-Fos (1:3000, SC-7202, Santa Cruz Biotechnology, USA). For detection of NeuN, DCX, and synaptophysin we used biotinylated secondary antibodies (Vector Laboratories) followed by processing with ABC kit (Vector Laboratories) and development with 2 mM diaminobenzidine (Sigma, USA) and 0.5 mM H_2O_2 in 0.1 M Tris buffer. Sections were put on gelatin-coated slides, air-dried overnight, dehydrated in graded solutions of ethanol, cleared in xylene, and mounted with Canada balsam. For GFAP immunohistochemistry, sections were incubated with anti-rabbit Alexa 488 (Invitrogen), put on gelatin-coated slides and mounted with PVA-DABCO (Sigma-Aldrich, USA).

Hippocampal Volume, Neuronal Counting, and Diameter Assessment

Total number of NeuN+ cells in CA1 pyramidal layer and granular cell layer (GCL) was quantified in coronal brain sections using the formula:

$$T = \frac{N * V}{t}$$

where N is the cell density, V is the volume of the structure, and t is the thickness of the section. The volume was calculated by measuring the area of the structure (pyramidal layer, GCL, or total hippocampus) with Optimas software and multiplying by section thickness, inter-section distance and number of sections. The diameter of NeuN+ cells in the GCL was estimated by measuring the area of at least 10 granular neurons per animal evenly sampling both blades of the DG. Areas (A) measured were approximated to a circle and cell diameter (D) was calculated using the formula:

$$D = \sqrt{4\frac{A}{\pi}}$$

DCX Counting in the Dentate Gyrus

Doublecortin (DCX) immunohistochemistry was used to study adult neurogenesis. Quantification of the number of DCX+ cells was done under a 40x objective in a Nikon E200 microscope. Every eighth 60 μm coronal brain section throughout the entire rostrocaudal extension of the DG were analyzed in each mouse ($n = 5$ per group). Cells were counted in the SGZ and in the GCL. Both upper and lower blades of the GCL and SGZ were considered for cell counting. Two DCX+ cell subpopulations were defined following a previously published classification (Beauquis et al., 2010). A less mature population (type A-D) corresponding to cells with not evident or short dendritic processes, with dendrites projecting parallel to the GCL longitudinal axis or presenting a dendritic tree not exiting the GCL. A second, more mature population (named E-F) included cells showing a primary dendrite that reached the molecular layer and a well-developed dendritic tree.

Synaptophysin Optical Density

Synaptophysin immunoreactivity was specifically quantified in the *stratum lucidum* region of CA3, to determine presynaptic densities corresponding to the contact between mossy fibers and CA3 pyramidal cells. Images of synaptophysin labeled sections were obtained under a 10X objective in a Nikon Eclipse E200 microscope. Optical density within the region of interest was measured using Optimas software and expressed as signal-to-background ratio.

Golgi Staining and Dendritic Spine Density

A modified osmium-free version of Golgi technique was used to study hippocampal pyramidal neurons (modified from Gonzalez-Burgos et al., 1992; Beauquis et al., 2010). After dissection, left brain hemispheres were immersed in 4% paraformaldehyde for 2 h and then transferred to a solution of 2.8 g/dL potassium dichromate in 8% formaldehyde diluted in distilled water for 48 h. After that, tissue was immersed overnight in a solution of 2.8 g/dL potassium dichromate in 2% formaldehyde and then in a solution of 3.5 g/dL potassium dichromate in distilled water where the tissue remained for 5 days. Then, impregnated tissue was incubated in silver nitrate 0.75 g/dL in distilled water for 48 h. All the preceding steps were done in the darkness and at RT. Finally, the tissue was stored in 30% sucrose at 4°C until coronal sectioning with a vibrating microtome at 200 μm (method modified from Gibb and Kolb, 1998). Sections were mounted on slides, pressed with blotting paper to avoid detachment during ethanol dehydration and xylene clearing, and coverslipped with Permount (Fisher Scientific). The density of dendritic spines was measured in pyramidal neurons in CA1. Using a Nikon Eclipse E200 microscope with 1250X magnification, dendritic spines were counted in secondary-order basal and apical dendrites. A minimum of 15 pyramidal neurons with at least 20-μm long dendritic segments in the same focal plane were sampled and results were expressed as number of spines per μm.

Astrocyte Number and Complexity Evaluation

The number of GFAP+ cells was quantified in CA1 hippocampal subfield using a modified version of the optical disector method as described in (Beauquis et al., 2013). Images of GFAP immunohistochemistry were acquired from *stratum*

radiatum and *lacunosum moleculare* in coronal brain sections, using a Nikon Eclipse E80 confocal microscope with a 40X air objective. Serial images were obtained along the *Z* axis (0.65-μm step) to generate a three-dimensional reconstruction (Z-stack) using NIH ImageJ software (Abramoff et al., 2004). Density of GFAP+ cells (number of cells/unit of volume) was quantified using a randomly placed 0.0024 mm^3 counting probe. A minimum of 100 cells was counted per animal and volume (*V*) of the analyzed regions was estimated using the Cavalieri principle on serial sections using the formula:

$$V = T\sum A$$

Areas (*A*) were measured using Optimas image analysis software and the *T* value was obtained by multiplying the number of sections by the distance between planes.

Complexity of GFAP+ astrocytes was calculated as the ratio between cell surface and volume. Both parameters were estimated on three-dimensional reconstructed images obtained from confocal *Z*-stacks using ImageJ software Cells entirely located inside the analyzed sections, presenting a complete staining and not overlapping with other cells or blood vessels were considered for counting. At least 25 cells evenly distributed across sections were analyzed per animal. A threshold was applied to images to exclude eventual unspecific staining prior to binarization. Cell surface (*S*) was estimated using the formula:

$$S = A_1 + A_n + \frac{d}{2}(P_1 + P_n) + d\sum_{i=2}^{n} p_i$$

Where $A_1 \ldots A_n$ and $p_1 \ldots p_n$ are the area and perimeter, respectively, of each image from the *Z*-stack and *d* represents the distance between sections. This formula is a modified version of the previously described by Chvàtal et al (Chvatal et al., 2007) and assumes that the progression of the surface and perimeter between planes of *Z*-stack is lineal in relation to the *Z* axis. The volume of individual GFAP+ cells was estimated using the Cavalieri principle as previously described.

c-Fos Positive Nuclei in Amygdala and Ventral Hippocampus

The number of c-Fos immunopositive cells was assessed in the central and basolateral amygdala and ventral hippocampus. Nuclei positive for c-Fos were counted under a 40x objective in a Nikon E200 microscope. c-Fos+ nuclei density (nuclei/mm^2) was quantified analyzing 63,523.02 μm^2 fields in central and basolateral amygdala and 14,400 μm^2 fields in the pyramidal layer of the ventral hippocampus from each brain section to obtain an average of c-Fos+ nuclei/mm^2.

Behavioral Procedures

Novel location recognition test

This test was performed in order to analyze hippocampus-dependent spatial memory (Revsin et al., 2009). Mice (NTg $n = 9$ and Tg $n = 8$) were tested in a black plastic box (30 x 30 x 30 cm^3) to which they were adequately habituated for 6 days prior to the trial. During the first day of habituation, all littermates where placed for 10 min in the box. For the following 5 days of habituation, each mouse was placed separately in the box for 5 min. The test consisted of two 10-min trials (sample trial or T1 and test trial or T2), that were recorded with a video camera, separated by a 1-h inter-trial interval. In T1, mice were exposed to two identical plastic objects that were placed in two selected contiguous corners, whereas during T2, one of the objects was moved to a novel location in the opposite corner respective to the nondisplaced object. Exploration of the objects was considered positive when the animals' nose was facing the objects less than 1 cm away from the object. Performance was assessed as the percentage of time exploring the object in the novel location to total exploration time in T2. Exploration of the objects in T1 was quantified in order to determine the correct habituation to the objects, establishing 20 s as the inclusion time criteria.

Open Field Test

An open field test was performed to evaluate exploratory behavior and anxiety. The apparatus consisted in a white wooden box (55 × 55 cm with 25 cm-high walls). Mice (NTg $n = 18$ and Tg $n = 12$) were placed in the center of the arena and behavior was analyzed for 5 min from video files. The arena was digitally divided into 25 equal squares (5×5) and 2 regions were defined: a central region comprising the inner 9 squares and a peripheral region corresponding to the outer 16 squares. The variables measured in this test were divided into quantitative and qualitative: line crossings (horizontal exploratory activity), rearings (vertical exploratory activity), and percent of time in the periphery were among the quantitative ones while defecation, reaction, and activity were the qualitative variables. "Activity" is a categorization of the quantitative variable "line crossings". Taking into account the median (195 line crossings), we considered values over the median as "high activity" and values below the median as "low activity". Likewise, the variable "reaction" was determined from the quantitative variable "movement," the time when the mouse first moves when placed in the center of the arena. Being the median one second, "rapid reaction" was established as one second or less, whereas "delayed reaction" occurred for more than 1 s.

Statistical Analysis

Data are expressed as mean ± SEM. Analyses were performed under blind condition to genotype. Statistical analyses were performed using unpaired one-tailed Student's *t* test and multivariate analysis when required in the open field test. Student's *t* tests were done using Prism 3.02 (GraphPad Software Inc.) while Info-Stat software (Universidad Nacional de Córdoba, Argentina) was used for multivariate analysis. Quantitative variables in the open field test were processed for multivariate analysis of variance followed by discriminant analysis.

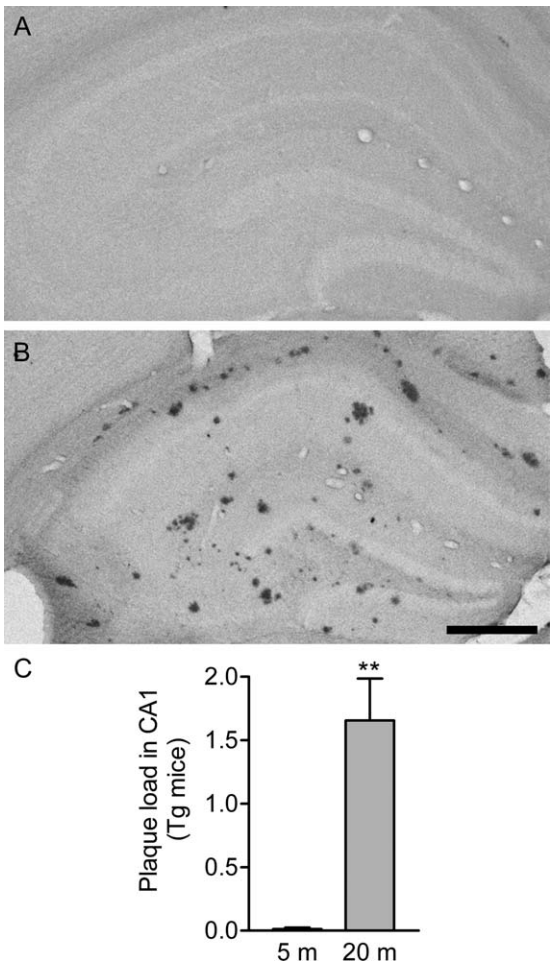

FIGURE 1. Absence of amyloid plaques on young PDAPP mice. Hippocampal amyloid deposition was analyzed in brain coronal sections after Congo red staining. Five-month-old animals (panel A) showed none or very few deposits. Brain sections from 20-month-old mice (panel B) were used in the same assay as positive controls, presenting abundant Congo red deposits throughout the hippocampus and cortex. The scale bar represents 300 μm. $^{**}P < 0.01$.

Briefly, this method creates a linear combination of the original variables which maximizes the difference between the groups defined prior to the analysis, called discriminant function. Coefficients of the discriminant function are an indicator of the importance of each variable in the discrimination of the groups. Information from qualitative variables was assessed with the correspondence analysis. This is a graphical technique that allows representing information given in a contingency table. A plot showing the interaction of the categories of each qualitative variable is constructed and its significance is tested using a chi-square test. Correspondence analysis creates canonical variables, which maximize the association of the categories in each variable. In all statistical analysis, the required assumptions for each test were verified and significant differences were considered at the 5% level and represented as P values ($P < 0.05$). Error bars in graphics represent the standard error.

RESULTS

Minimal Amyloid Deposition on Hippocampus from 5-Month-Old PDAPP Mice, with Low Brain Levels of Aβ 1–40 and 1–42 APP Derived Peptides

Hippocampal amyloid load was determined on brain sections from Tg mice using Congo red staining (Fig. 1). Specific staining of amyloid deposits with Congo red was confirmed by performing an immunohistochemistry for amyloid β (4G8 antibody, MAB1561, Chemicon) in parallel sections from the same animals, yielding similar plaque counts (not shown). As it was recently reported in a previous work of our group (Beauquis et al., 2013) Congo red-stained sections were preferred to quantify plaque load as they provided a higher specific signal/background ratio than immunohistochemistry. In both cases no plaques or few incipient deposits were detected in Tg mice at 5 months of age (Fig. 1A). Twenty-month-old positive control mice showed abundant amyloid deposits (plaque load 1.656 ± 0.32 for Tg 20 m vs. 0.011 ± 0.01 for Tg 5 m; $P < 0.001$; Fig. 1B, C). Aβ1–40 and 1–42 APP-derived peptide levels quantified by specific ELISA were also low in Tg mice and were not detected in control animals (Table 1).

Early Hippocampal, CA1 and Dentate Gyrus Volume Reduction. Fewer Granular and CA1 Pyramidal Neurons. Decreased Cell Diameter in Young PDAPP Mice

We investigated a potential variation in the hippocampus volume from 5-month-old transgenic mice. An accurate hippocampal volume measurement after NeuN immunohistochemistry showed a 14.3% decline in the Tg group respect to NTg (9.583 ± 0.244 mm^3 in NTg mice vs. 8.210 ± 0.405 mm^3 in Tg mice; $P < 0.01$; Figs. 2A,B). Also, the volume of CA1 subfield from Tg mice differed from NTg group, showing a significant reduction near to 27% (0.365 ± 0.028 mm^3 in NTg vs. 0.266 ± 0.028 mm^3 in Tg; $P < 0.05$; Fig. 2C) while the volume of the GCL decreased 28% (0.519 ± 0.021 vs. 0.374 ± 0.034 mm^3 in NTg and Tg group respectively; $P < 0.01$; Fig. 2D). These volume reductions were accompanied by decreased number of neurons in CA1 and DG (Figs. 2E,F). The number of pyramidal neurons from CA1 subfield was decreased in the Tg group by 26% ($62{,}740 \pm 5{,}369$ cells

TABLE 1.

Brain Concentration of Human Aβ 1–40 and 1–42 Peptides

	NTg	T_g
Aβ 1–40 peptide (ng/g tissue)	ND	0.525 ± 0.308 ($n = 7$)
Aβ 1–42 peptide (ng/g tissue)	ND	1.264 ± 0.751 ($n = 7$)

Human Aβ 1–40 and 1–42 peptides were determined by specific ELISA assay in young PDAPP mice hemi-brain homogenates. ND, not detected.

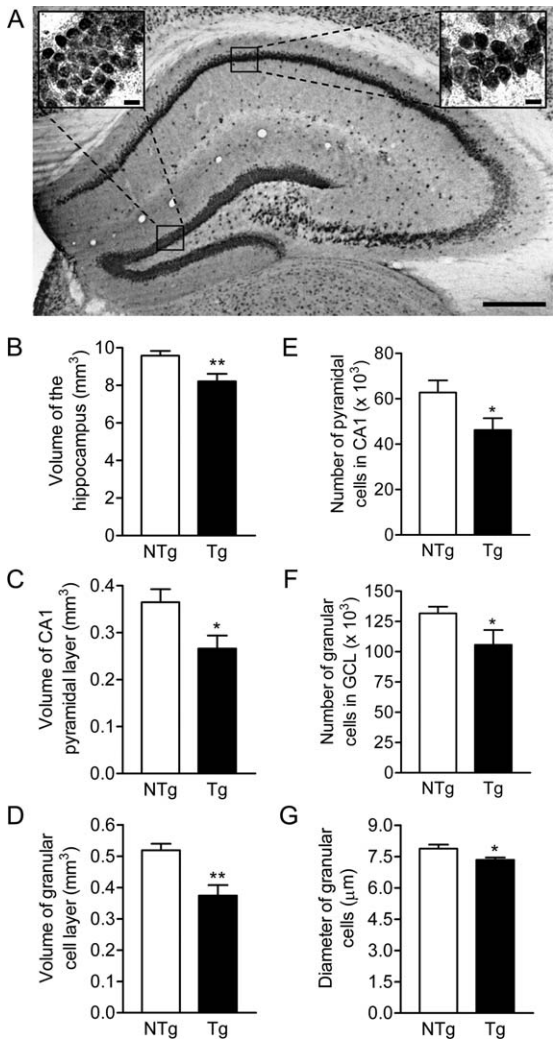

FIGURE 2. Hippocampal volume and neuronal alterations in PDAPP-J20 mice. Panel A shows a representative image of a coronal brain section containing hippocampus processed for NeuN immunohistochemistry (scale bar represents 300 μm). Insets show the soma of granule cells and CA1 pyramidal cells positive for NeuN at higher magnification (scale bar represents 10 μm). The volume of whole hippocampus (B) was found diminished in Tg mice respect to NTg littermates ($n = 5$ in each group). Also, a volume reduction in CA1 pyramidal layer and granular cell layer (GCL) was detected in the Tg group (C and D). As show in panels E and F, the volume reduction of these regions was associated with less number of pyramidal and granular neurons in CA1 and GCL respectively. This effect was accompanied by a reduction in the diameter of the soma of granular cells in Tg mice (G). *$P < 0.05$ and **$P < 0.01$.

in NTg vs. 46,200 ± 5,247 cells in Tg; $P < 0.05$) whereas the number of granular neurons in the GCL was reduced by 19.7% when compared with the NTg group (13,1700 ± 5,583 vs. 10,5700 ± 1,229 cells in NTg and Tg mice respectively; $P < 0.05$). In addition to the decreased number of granule neurons, a 7% reduction in granule cell diameter was also found in Tg mice (7.882 ± 0.200 and 7.335 ± 0.120 μm in NTg and Tg mice, respectively; $P < 0.05$; Fig. 2G). Neuronal diameter estimation was statistically similar using both Nissl staining (not shown) and NeuN immunolabeling.

Marked Decrease in Neurogenesis in the Dentate Gyrus of Young PDAPP Mice

In order to study the neurogenic status of young PDAPP-J20 mice, we counted the number of doublecortin+ (DCX) newborn neurons in the DG (Figs. 3A–C). The number of DCX+ cells in the dorsal and ventral DG was significantly lower in the PDAPP mice compared with age-matched controls (2,727 ± 360.3 vs. 6,585 ± 432.2, number of DCX+ cells in the DG of Tg and NTg mice respectively; $P < 0.0001$). The neuronal population exhibiting DCX immunostaining is heterogeneous in the DG, ranging from neuroblasts to young ~20-day-old neurons, presenting different stages of development. After this time window, the neurons become DCX-. We divided these stages into two categories: A-D, where the earliest stages are included, and E-F, comprising more mature neurons with DCX+ secondary dendrites exiting the GCL. Nontransgenic mice showed a predominant proportion of A-D (60.55%) neurons. Conversely, in Tg mice we found a significant increase in the percentage of neurons showing a mature morphology (55.35% E-F) in detriment of those in the early stage ($P < 0.05$ vs. NTg).

Reduced CA3 Synaptophysin Optical Density in 5-Month-Old AD Mice

We studied neuronal connectivity in the CA3 hippocampal subfield by analyzing synaptophysin immunoreactivity (Figs. 3D–F). Optical density of immunopositive areas was measured in the *stratum lucidum* of CA3 and a score was calculated to correct for background optical density. A significant decrease in the expression of synaptophysin was found in Tg mice compared with controls (0.136 ± 0.016 and 0.084 ± 0.019 for NTg and Tg, respectively; $P < 0.05$).

No Changes in CA1 Dendritic Spine Density in Young AD Mice Compared with Controls

Spine density was calculated in dendrites from CA1 pyramidal neurons in Golgi-stained hemi-brains (Figs. 3G–I). The number of spines per μm regardless of their morphology did not change between NTg and Tg groups (0.922 ± 0.031 vs. 0.937 ± 0.056).

Increased c-Fos+ Neuronal Activation in the Amygdala of Tg Mice. No Changes in Ventral Hippocampus

Immunohistochemical detection of Fos, the protein product of the immediate early gene c-fos, was evaluated as a functional marker linked to neural activity of central and basolateral amygdala, brain region intimately related to emotions and fear (Figs. 3J–L). c-Fos+ nuclei density (nuclei/mm^2) was found to be augmented in Tg mice (241.4 ± 29.93 vs. 145.1 ± 12.06, $P < 0.01$). However, the c-Fos density measured in the ventral

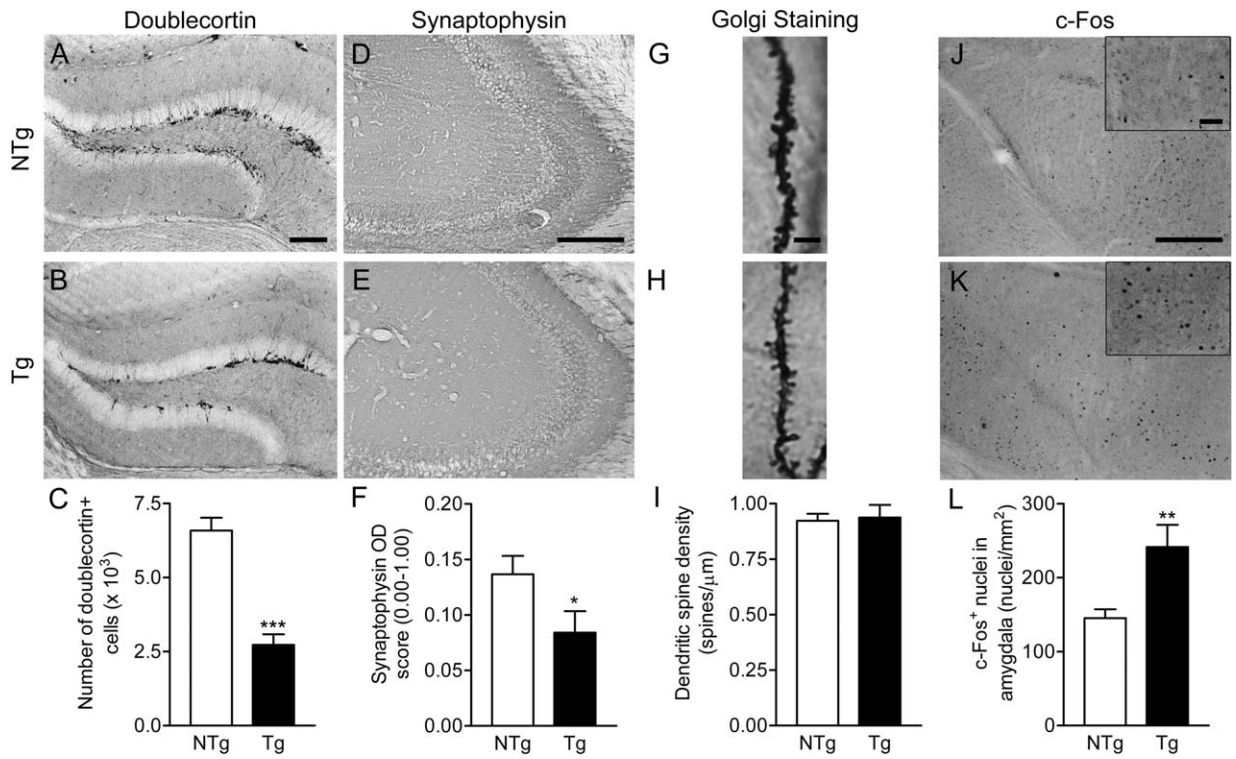

FIGURE 3. Neurogenesis, synaptic density and neuronal activity in 5-month-old PDAPP mice. Panels A and B show representative images from DCX immunohistochemistry in the dentate gyrus of NTg (A) and Tg (B) mice (scale bar represents 150 μm) Transgenic mice showed a decreased number of DCX+cells in the DG (panel C). Panels D and E show images of CA3 stratum lucidum immunostained for synaptophysin (scale bar represents 200 μm). Optical density score for synaptophysin was found to be reduced in Tg mice (panel F). Spine density of CA1 pyramidal neurons was quantified in Golgi-stained brain sections (panels G an H; scale bar represents 5 μm) and did not vary significantly between strains (I). c-Fos immunoreactivity in central and basolateral amygdala (panels J and K; scale bar represents 150 μm in main images and 50 μm in both insets) denoted a hyper-activation of amygdala nuclei in Tg mice (panel L). *$P<0.05$, **$P<0.01$, and ***$P<0.0001$.

hippocampus corresponding to CA1 subfield showed no changes between experimental groups (Tg 756.94 ±70.66; NTg 811.11±63.20 nuclei/mm^2; $P<0.58$).

Decreased Number and Cell Complexity of GFAP+ Astrocytes in the Hippocampus of AD Mice Compared with Age-Matched Controls

Number of GFAP+ cells in CA1 *stratum radiatum* (Fig. 4A) was calculated as the product between GFAP+ cell density (cells/mm^3) and the volume of the region. This quantification was done on an averaged and inverted image of *z*-stacked confocal images. The number of cells was markedly reduced in Tg mice in absence of amyloid plaques (16,120 ± 671 GFAP+ cells in NTg group vs. 11,820 ± 1,033 GFAP+ cells in Tg group; $P<0.01$). Complexity of GFAP+ astrocytes was evaluated as the index resulting from the ratio between surface and volume of each cell (Figs. 4B–E). To accomplish this, each GFAP+ cell was individually reconstructed integrating serial confocal images and calculating both parameters as described in material and methods section. Using this method, morphological alterations were found in GFAP+ astrocytes from Tg mice, showing a decrease in the complexity index respect to controls (68.19 ± 3.80 vs. 53.01 ± 2.72 in NTg and Tg respectively; $P<0.01$). It must be noted that no changes were detected neither in surface or volume individually, but the ratio between these variables was significantly altered.

Impairment of Hippocampus-Dependent Spatial Memory in Transgenic Mice

Hippocampus-dependent spatial memory was evaluated conducting the novel location recognition test using a 1-h intertrial interval (Fig. 5A). Mice were habituated to the test arena for 6 days prior to the evaluation. A 20-s exploration time was adopted as the inclusion criteria. No significant differences in the T1 exploration time were found between groups (46.89 ± 4.53 s and 46.49 ± 7.18 s for NTg and Tg respectively; $P=0.96$), guarantying equivalent learning opportunity for every mouse. Exploration time in T1 was equivalent for both identical objects in both groups (NTg 48.89 ± 0.88 and 51.11 ± 0.88 %T1; $P=0.11$; Tg 50.97 ± 1.08 and 49.03 ± 1.07 %T1; $P=0.24$), denoting no location preference. Total exploration time of both objects in T2 was

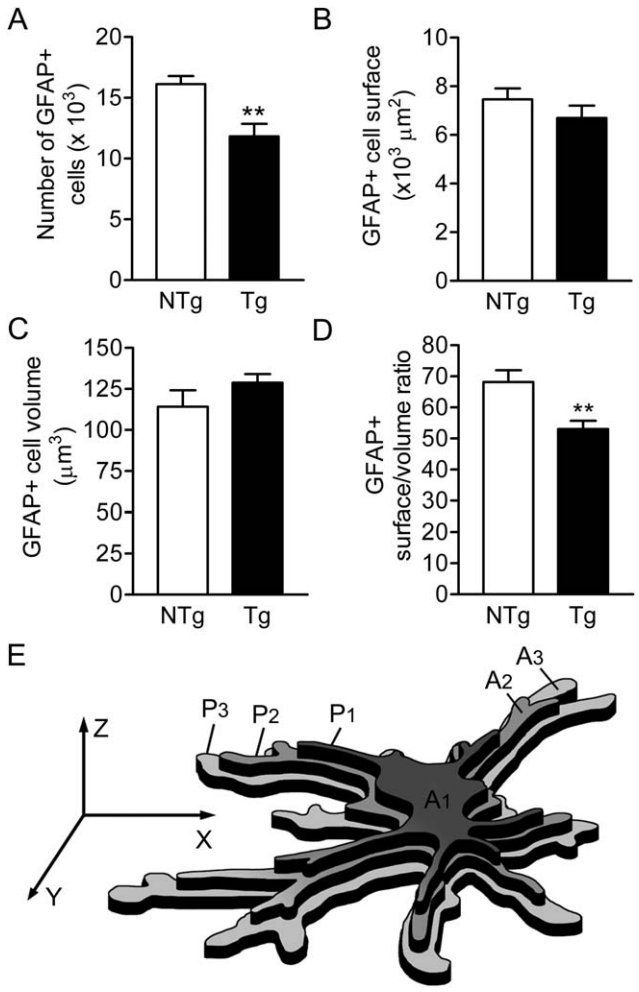

FIGURE 4. Morphological alterations of GFAP+ cells in the hippocampus of PDAPP-J20 mice. Panel A shows the total number of GFAP+ cells in CA1 stratum radiatum, with Tg mice showing a decrease compared with control mice, Using z-stacked confocal images, GFAP+ volume and total surface of individual cells (panels B and C) was calculated from the perimeter (P) and area (A) of each image (panel E) but no differences were found between experimental groups. Cell complexity index (surface/volume ratio) of individual GFAP+ astrocytes (panel D) was found diminished in Tg mice. Cell volume was calculated assuming that the GFAP+ cell area does not change between planes of consecutives images in the *z*-stack, as shown in panel E. On the other hand, single-cell total surface was calculated assuming that GFAP+ area changes linearly between consecutive images of the Z-stack. **$P < 0.01$.

equivalent for both groups (35.26 ± 3.92 s and 34.40 ± 3.59 s for NTg and Tg, respectively; $P = 0.87$). Transgenic mice spent less percent of the exploration time in T2 exploring the relocated object than control mice (67.60 ± 2.81% and 54.18 ± 3.26% for NTg and Tg, respectively; $P < 0.01$). Also, a one-sample *t* test was done to determine differences between percentual exploration time of the relocated object and a theoretical mean of 50% representing the chance level for this test, i.e., the probability of randomly exploring both objects. Values in control mice were significantly different from chance level whereas Tg mice not ($P < 0.001$ vs. chance level for NTg mice and $P = 0.24$ for Tg mice; Fig. 5B).

Transgenic Mice Exhibited Increased Anxiety Compared with Control Mice

To investigate the behavioral performance in the Open Field test, we discriminated several factors including number of rearings, percent of time spent in the periphery of the arena and number of line crossings during the 5-min test (Supporting Information, Table 1). The mean of the discriminant function was negative for NTg (−0.51±0.26) and positive for Tg mice (0.76±0.23) and significantly differed between groups ($P < 0.05$; Fig. 5C). The discriminant function acquired a positive value when associated to decreased rearings, increased crossings and more % of time in the periphery.

For the implementation of the correspondence analysis (Fig. 5D), canonical axes were extracted according to the fraction of the association that they represent. The first two canonical axes represented 63% of the association between variables (35.8% for canonical axis 1 and 27.2% for canonical axis 2). Canonical variables showed that Tg mice were associated with "high activity," "delayed reaction" and "defecation" ($P < 0.05$).

DISCUSSION

Early Structural and Neural Alterations in the Hippocampus of Young AD Mice

There is a large consensus about the imperative necessity to identify early targets and characterize premature symptoms in the progression of Alzheimer's disease (AD). In this study, we found multiple neural and glial changes in the hippocampus of PDAPP-J20 mice at a preplaque stage of disease progression. We have chosen to study this strain punctually at the age of 5-month-old because at this time point there is no significant amyloid deposition and the levels of Aβ-APP derived peptides in the brain homogenates are scarcely detectable. Congo red staining, confirmed with specific immunohistochemistry against Aβ, revealed the absence of senile plaques in the hippocampus and cortex of 5-month-old PDAPP-J20 mice while Aβ 1–40 and 1–42 levels, assessed by ELISA in hemi-brain guanidine homogenates, were measurable but barely above the detection limit. As no plaques were found at this age, the source of Aβ levels could be considered mostly Aβ oligomer soluble fraction, which have known neurotoxic effects (Larson and Lesne, 2012).

The notion that normal brain aging is accompanied by histological and anatomical morphological changes that strongly differ from AD brain alterations was established some years ago using magnetic resonance imaging in patients and control subjects (Ohnishi et al., 2001). Interestingly, chronic neuropsychiatric illnesses can be diagnosed analyzing brain images, suggesting the existence of a distinctive morphostructural

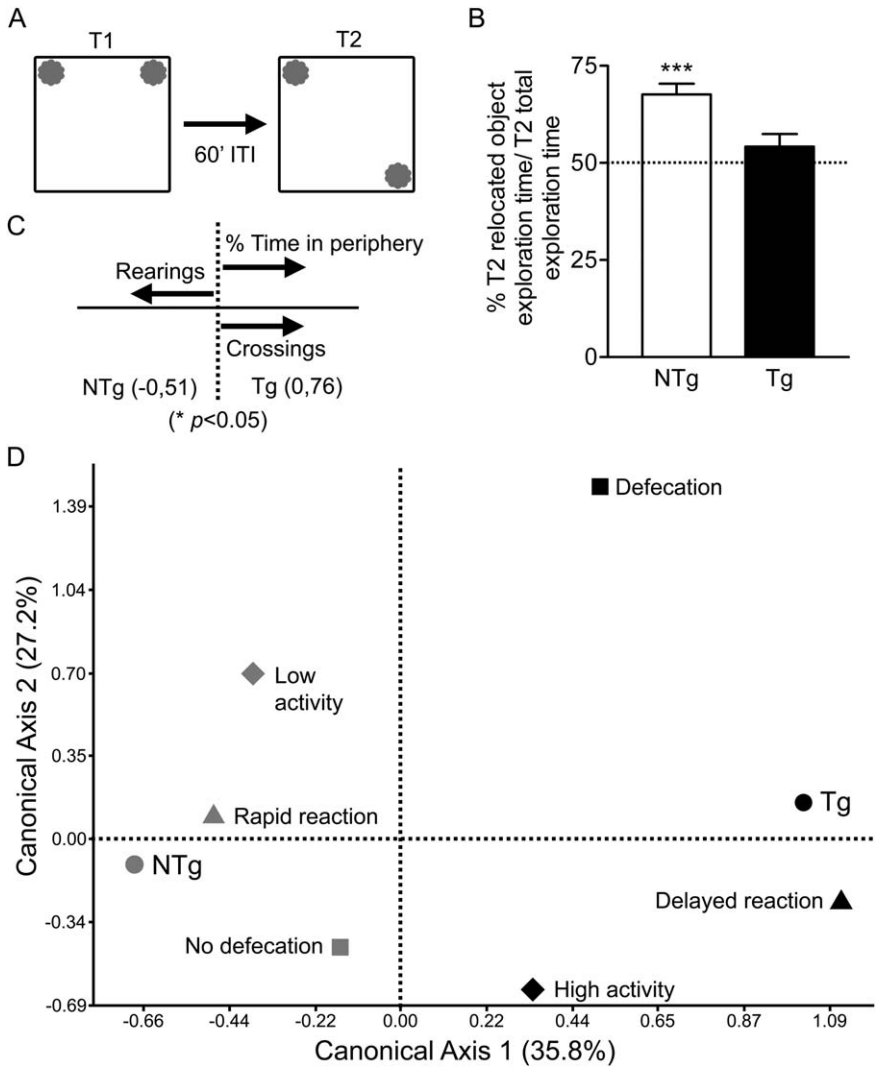

FIGURE 5. Behavioral profile: spatial memory impairment and increased anxiety. Panel A schematizes trial 1 and trial 2 of the novel location recognition test and object disposition. Panel B shows mice performance expressed as the percent of total T2 time that was employed to explore the relocated object. NTg mice significantly spent more time exploring the newly located object while Tg mice explored both objects randomly (*$P < 0.001$ and $P = 0.24$ vs. 50% theoretical mean for NTg and Tg mice, respectively). Multivariate analysis of the open-field test (panel C) showed that the discriminant function in Tg mice was related to less rearings, more line crossings, and greater time in the periphery of the arena. The correspondence analysis (panel D) demonstrated that Tg mice were associated to delayed reaction, high activity and defecation, while NTg mice were associated to rapid reaction, low activity, and no defecation ($P < 0.05$).**

pattern associated to each disease (Bansal et al., 2012). In this work, hippocampal volume from Tg mice was reduced by 12% compared with the control group. This volume loss was also verified and more prominent in CA1 (28% reduction) and DG (25% reduction). These changes in the DG at early phases of the disease are in accordance with a magnetic resonance microscopy study where the volume of the DG was found decreased in the same transgenic mice model (Redwine et al., 2003). Using stereological tools we found that this volume loss was associated with a significantly decreased density of NeuN+ cells in both subfields. Moreover, cell diameter of granular neurons was affected in the Tg group, showing a reduction that was near 10% compared with control values. Previous reports in the literature give strong evidence about the loss of neurons associated to the neurodegenerative process in post mortem brains from AD patients, with emphasis in CA1 vulnerability (West et al., 2000). Even if there is no total consensus about loss of neurons in AD models, some studies corroborated this finding in the PDAPP mouse (Wright et al., 2013). However, to the best of our knowledge, few reports informed neuronal atrophy (van de Nes et al., 2008; Gemmell et al., 2012). Analyzing pyramidal neurons in post mortem brains from patients with AD and other dementias, Gemmell et al. referred decreased hippocampal neuronal volume that correlated with

cognitive deficits (Gemmell et al., 2012). Consistent with these findings, we observed a significant reduction of granular cell volume in the DG of young AD mice that could reflect a potential dendritic dysfunction and/or an initial step in neuronal death. Using DCX immunohistochemistry we detected a marked decline in adult hippocampal neurogenesis in Tg mice compared with controls, reinforcing the idea of impaired connectivity or disruption of hippocampal circuitry. Even if there are some punctual discrepancies in the literature about the neurogenic status in AD, this is in part due to differences in the time-point of disease progression analyzed, in the animal model evaluated and the cell marker used to explore neurogenesis (Jin et al., 2004; Lilja et al., 2013). In this study, not only the number of DCX+ cells was significantly decreased in Tg mice but also morphological maturation of these cells differed from those in healthy controls, suggesting that soluble APP-derived peptides, already present at this age, could interfere with the time course of adult neurogenesis.

Brain neurodegeneration and, specifically, AD are strongly associated with loss of synaptophysin+ densities (Brun, 2007) and, in PDAPP-J20 mice, behavioral impairments are intimately linked to synaptic transmission deficits (Galvan et al., 2006). In our study, we found a decrease in pre-synaptic synaptophysin optical density in the *stratum lucidum* of CA3 subfield, area where mossy fibers from granule cells of the DG contact pyramidal cells, denoting precocious damage of the hippocampal circuitry before the establishment of overt amyloid pathology. Largely, the excitatory input in the hippocampus impinges on dendritic spines that are crucial for neural processing, being spine density a reflect of changes in the strength of synaptic transmission (Bohlen Und, 2009). Numerous studies analyzing human postmortem tissue, animal models, and cellular paradigms indicate that advanced AD pathology has a damaging effect on the pathways governing actin cytoskeleton stability (Penzes and Vanleeuwen, 2011), but not much is known about spine density on early pathological stages. Various authors informed loss of dendritic spines in transgenic mouse models at middle or advanced stages of the pathology (Moolman et al., 2004; Perez-Cruz et al., 2011). However, at 5 months of age, the dendritic spine density from CA1 pyramidal neurons in Tg mice, studied by Golgi staining, was not significantly altered. Preliminary data from our lab show a considerable decrease in pyramidal spine density 3 months later, at 8 months of age in the Tg group (unpublished data), possibly suggesting that further disease progression is required for CA1 synaptic damage to be evidenced.

Less Astrocytes and Reduced Cell Complexity in the Hippocampus of Young PDAPP Mice

There is an agreement about the astrogliosis event accompanying the neurodegenerative process in AD and other diseases (Vijayan et al., 1991; Heneka et al., 2010; Verkhratsky et al., 2012). Two astroglial populations have been described at moderate and advanced stages: hyper-reactive astrocytes surrounding amyloid deposits and, more recently, astrocytes not associated to amyloid plaques exhibiting a marked decrease of cell complexity and volume compared with control values (Bansal et al., 2012; Parpura and Verkhratsky, 2012) The expression of GFAP is strongly augmented in correlation with disease progress in different AD mouse models (Galvan et al., 2006; Kamphuis et al., 2012). As our data show, the number of GFAP+ astrocytes can be affected in the hippocampus, even at an early stage of the pathology, in association with changes in astrocyte complexity, evaluated as the ratio between area and volume of each cell. The literature is not consistent about the number and reactivity of GFAP+ cells in the AD brain. To consider the reported data it is necessary to distinguish not only between different AD models used but also, and more importantly, disease progression and methods applied for cell analysis. For instance, in apparent contradiction with our results, Wright and co-workers reported an increase in the GFAP+ astroglial population starting at 12 weeks of age in the CA1 region from PDAPP-J20 mice (Wright et al., 2013). However, this result represents the estimation of astrocyte number obtained without association to regional volume, differing with the method we applied. In a recent publication, we explored the impact of enriched environment on astroglial morphology in PDAPP mice, among other points. In that work, the cellular volume of GFAP+ astrocytes from 5-month-old mice did not vary between Tg and NTg group (Beauquis et al., 2013). In the present morphological characterization study, we added the complexity index to detect subtle cell changes and we found it significantly decreased in astrocytes from Tg mice. Shortening and simplification of astroglial processes may be reflected by subtle alterations in volume and cell surface that could represent early astrocyte activation in this animal model at an age when there are no manifest signs of amyloid deposition. Morphological and structural changes found in hippocampal astrocytes could indicate an early loss of supporting function and increased neuronal vulnerability. Focusing on morphology, Rodriguez et al. found reduced complexity in astroglial cytoskeleton from 3xTgAD mice compared with matching controls but the difference was only significant at 12 months of age (Rodriguez et al., 2009). A similar result was found in post-mortem brains from dementia patients (Senitz et al., 1995). Both, reactive astrocytes close to deposits and dysfunctional astrocytes away from amyloid lesions could provide less support to neurons, provoking progressive neuronal dysfunction and death.

Cognitive Deficit and Increased Anxiety Index Before Amyloid Deposition. Involvement of Emotionality from Initial AD Stages

We chose behavioral tests to assess hippocampal-dependent spatial memory and behavioral variables involved in an anxious phenotype, avoiding physically demanding and stressful tasks. Transgenic mice exhibited a poor performance in the novel location recognition task compared with controls. As it is well established, memory for an object location is strongly dependent on hippocampal integrity, although contextual associations

depend also on perirhinal and medial prefrontal cortex interactions (Ennaceur et al., 1996; Barker and Warburton, 2011). Cognitive deficits have been described in AD murine models, but most results are associated to advanced progression of the neurodegenerative process (Wright et al., 2013). However, Taglialatela et al. found impaired performance in the novel object recognition test in 5-month-old Tg2576 mice though only when the retention interval was prolonged for at least 4 h, showing a long-term recognition deficit (Taglialatela et al., 2009). Our results, showing compromised performance in the novel location recognition test in young Tg mice, with a 1-h retention interval, might be associated with the impairment of adult hippocampal neurogenesis evidenced by DCX+ immunohistochemistry, given the potential role of adult-born neurons in spatial learning (Marin-Burgin and Schinder, 2012). Punctually, Goodman et al. reported an association of young hippocampal neurons with recent and remote spatial memory using cytostatic agents to reduce neurogenesis in mice and hippocampus-dependent and independent tasks (Goodman et al., 2010).

In addition, the loss of CA3 synaptophysin density as well as the drop in the number of neurons and astrocytes found prematurely in Tg mice could also underlie cognitive deficits. Further studies are required to establish whether this early cognitive impairment affects also long-term memory and to discriminate between the different stages involved in the memory process (acquisition, consolidation, retention, and retrieval).

Anxious behavior was recently suggested as a key factor increasing the risk for aging diseases in both, humans and rodents (O'Donovan et al., 2013) and inflammation was signaled as an important player. Applying a multivariate statistical analysis to the behavioral outcome of the open-field test, we found an anxious phenotype associated with a marked c-Fos neuronal activation in the central and basolateral amygdala in Tg mice. This increase in the number of c-Fos+ cells was not found in the ventral hippocampus, suggesting an amygdala-specific effect at the studied age. Multivariate statistical analysis of behavioral variables allowed us to develop an anxiety index that increased the sensitivity of the test. Though, when these behavioral variables were analyzed separately, differences were found only in the percent of time in the periphery. For instance, Wright et al reported an increase in total distance traveled in PDAPP mice starting at 18-weeks of age; however, time spent in open arms in the elevated plus maze did not differ from controls even later (Wright et al., 2013). Multivariate analyses are relevant in conduct evaluation as, in many cases, a single variable is not sufficient to describe a complex behavior. Tests such as multivariate analysis of variance and correspondence analysis, are strongly recommended in the bibliography to analyze this kind of studies (Leighty et al., 2004; Arendash et al., 2004).

To conclude, in this study we have identified important structural and morphological alterations in the hippocampus of young PDAPP-J20 mice preceding the presence of amyloid deposits though APP derived peptides levels were detectable but at very low levels. With focus on neurons and astroglia we detected not only a premature loss of both cell populations, but also changes in neuronal diameter and astrocyte complexity, which could constitute early indicators of the disease. The question that remains still open refers to the founding phenomena that could signal the beginning of the disease. Further studies on early post natal alterations and/or embryonic involvement are in course in order to address this issue. It would be interesting to explore whether these early neuroglial changes correlate with precocious brain alterations in AD or mild cognitive impairment patients.

Acknowledgments

The authors thank Pablo Pomata for his assistance with confocal microscopy and the personnel of the animal facility at the Instituto de Biología y Medicina Experimental (IBYME) for their help with animal care. JB and FS are career investigators from Consejo Nacional de Investigaciones Científicas y Técnicas of Argentina (CONICET).

REFERENCES

Abramoff MD, Magelhaes PJ, Ram SJ. 2004. Image Processing with ImageJ. Biophotonics International 11:36–42.

Albert MS. 2011. Changes in cognition. Neurobiol Aging 32 (Suppl 1):S58–S63.

Arendash GW, Garcia MF, Costa DA, Cracchiolo JR, Wefes IM, Potter H. 2004. Environmental enrichment improves cognition in aged Alzheimer's transgenic mice despite stable beta-amyloid deposition. Neuroreport 15:1751–1754.

Bansal R, Staib LH, Laine AF, Hao X, Xu D, Liu J, Weissman M, Peterson BS. 2012. Anatomical brain images alone can accurately diagnose chronic neuropsychiatric illnesses. PLoS One 7:e50698.

Barker GR, Warburton EC. 2011. When is the hippocampus involved in recognition memory? J Neurosci 31:10721–10731.

Beauquis J, Pavia P, Pomilio C, Vinuesa A, Podlutskaya N, Galvan V, Saravia F. 2013. Environmental enrichment prevents astroglial pathological changes in the hippocampus of APP transgenic mice, model of Alzheimer's disease. Exp Neurol 239:28–37.

Beauquis J, Roig P, De Nicola AF, Saravia F. 2010. Short-term environmental enrichment enhances adult neurogenesis, vascular network and dendritic complexity in the hippocampus of type 1 diabetic mice. PLoS One 5:e13993.

Blennow K, de Leon MJ, Zetterberg H. 2006. Alzheimer's disease. Lancet 368:387–403.

Bohlen Und HO. 2009. Structure and function of dendritic spines within the hippocampus. Ann Anat 191:518–531.

Brun A. 2007. Identification and characterization of frontal lobe degeneration: Historical perspective on the development of FTD. Alzheimer Dis Assoc Disord 21:S3–S4.

Chvatal A, Anderova M, Hock M, Prajerova I, Neprasova H, Chvatal V, Kirchhoff F, Sykova E. 2007. Three-dimensional confocal morphometry reveals structural changes in astrocyte morphology in situ. J Neurosci Res 85:260–271.

Dubois B, Feldman HH, Jacova C, Cummings JL, DeKosky ST, Barberger-Gateau P, Delacourte A, Frisoni G, Fox NC, Galasko D, et al. 2010. Revising the definition of Alzheimer's disease: A new lexicon. Lancet Neurol 9:1118–1127.

Ennaceur A, Neave N, Aggleton JP. 1996. Neurotoxic lesions of the perirhinal cortex do not mimic the behavioural effects of fornix transection in the rat. Behav Brain Res 80:9–25.

Galvan V, Gorostiza OF, Banwait S, Ataie M, Logvinova AV, Sitaraman S, Carlson E, Sagi SA, Chevallier N, Jin K, et al. 2006. Reversal of Alzheimer's-like pathology and behavior in human APP transgenic mice by mutation of Asp664. Proc Natl Acad Sci USA 103:7130–7135.

Gemmell E, Bosomworth H, Allan L, Hall R, Khundakar A, Oakley AE, Deramecourt V, Polvikoski TM, O'Brien JT, Kalaria RN. 2012. Hippocampal neuronal atrophy and cognitive function in delayed poststroke and aging-related dementias. Stroke 43:808–814.

Gibb R, Kolb B. 1998. A method for vibratome sectioning of Golgi-Cox stained whole rat brain. J Neurosci Methods 79:1–4.

Gonzalez-Burgos I, Tapia-Arizmendi G, Feria-Velasco A. 1992. Golgi method without osmium tetroxide for the study of the central nervous system. Biotech Histochem 67:288–296.

Goodman T, Trouche S, Massou I, Verret L, Zerwas M, Roullet P, Rampon C. 2010. Young hippocampal neurons are critical for recent and remote spatial memory in adult mice. Neuroscience 171:769–778.

Heneka MT, Rodriguez JJ, Verkhratsky A. 2010. Neuroglia in neurodegeneration. Brain Res Rev 63:189–211.

Hsia AY, Masliah E, McConlogue L, Yu GQ, Tatsuno G, Hu K, Kholodenko D, Malenka RC, Nicoll RA, Mucke L. 1999. Plaque-independent disruption of neural circuits in Alzheimer's disease mouse models. Proc Natl Acad Sci U S A 96:3228–3233.

Irizarry MC, Soriano F, McNamara M, Page KJ, Schenk D, Games D, Hyman BT. 1997. Abeta deposition is associated with neuropil changes, but not with overt neuronal loss in the human amyloid precursor protein V717F (PDAPP) transgenic mouse. J Neurosci 17:7053–7059.

Jin K, Galvan V, Xie L, Mao XO, Gorostiza OF, Bredesen DE, Greenberg DA. 2004. Enhanced neurogenesis in Alzheimer's disease transgenic (PDGF-APPSw,Ind) mice. Proc Natl Acad Sci USA 101:13363–13367.

Kamphuis W, Mamber C, Moeton M, Kooijman L, Sluijs JA, Jansen AH, Verveer M, de Groot LR, Smith VD, Rangarajan S, et al. 2012. GFAP isoforms in adult mouse brain with a focus on neurogenic astrocytes and reactive astrogliosis in mouse models of Alzheimer disease. PLoS One 7:e42823.

Larson ME, Lesne SE. 2012. Soluble Abeta oligomer production and toxicity. J Neurochem 120(Suppl 1):125–139.

Leighty RE, Nilsson LN, Potter H, Costa DA, Low MA, Bales KR, Paul SM, Arendash GW. 2004. Use of multimetric statistical analysis to characterize and discriminate between the performance of four Alzheimer's transgenic mouse lines differing in Abeta deposition. Behav Brain Res 153:107–121.

Lilja AM, Rojdner J, Mustafiz T, Thome CM, Storelli E, Gonzalez D, Unger-Lithner C, Greig NH, Nordberg A, Marutle A. 2013. Age-dependent neuroplasticity mechanisms in Alzheimer Tg2576 mice following modulation of brain amyloid-beta levels. PLoS One 8: e58752.

Marin-Burgin A, Schinder AF. 2012. Requirement of adult-born neurons for hippocampus-dependent learning. Behav Brain Res 227: 391–399.

Moolman DL, Vitolo OV, Vonsattel JP, Shelanski ML. 2004. Dendrite and dendritic spine alterations in Alzheimer models. J Neurocytol 33:377–387.

Mucke L, Masliah E, Yu GQ, Mallory M, Rockenstein EM, Tatsuno G, Hu K, Kholodenko D, Johnson-Wood K, McConlogue L. 2000. High-level neuronal expression of abeta 1–42 in wild-type human amyloid protein precursor transgenic mice: Synaptotoxicity without plaque formation. J Neurosci 20:4050–4058.

O'Donovan A, Slavich GM, Epel ES, Neylan TC. 2013. Exaggerated neurobiological sensitivity to threat as a mechanism linking anxiety with increased risk for diseases of aging. Neurosci Biobehav Rev 37:96–108.

Ohnishi T, Matsuda H, Tabira T, Asada T, Uno M. 2001. Changes in brain morphology in Alzheimer disease and normal aging: Is Alzheimer disease an exaggerated aging process? AJNR Am J Neuroradiol 22:1680–1685.

Palop JJ, Chin J, Roberson ED, Wang J, Thwin MT, Bien-Ly N, Yoo J, Ho KO, Yu GQ, Kreitzer A and others. 2007. Aberrant excitatory neuronal activity and compensatory remodeling of inhibitory hippocampal circuits in mouse models of Alzheimer's disease. Neuron 55:697–711.

Palop JJ, Mucke L. 2009. Epilepsy and cognitive impairments in Alzheimer disease. Arch Neurol 66:435–440.

Parpura V, Verkhratsky A. 2012. Neuroglia at the crossroads of homeostasis, metabolism and signaling: Evolution of the concept. ASN Neuro .

Penzes P, Vanleeuwen JE. 2011. Impaired regulation of synaptic actin cytoskeleton in Alzheimer's disease. Brain Res Rev 67:184–192.

Perez-Cruz C, Nolte MW, van Gaalen MM, Rustay NR, Termont A, Tanghe A, Kirchhoff F, Ebert U. 2011. Reduced spine density in specific regions of CA1 pyramidal neurons in two transgenic mouse models of Alzheimer's disease. J Neurosci 31:3926–3934.

Redwine JM, Kosofsky B, Jacobs RE, Games D, Reilly JF, Morrison JH, Young WG, Bloom FE. 2003. Dentate gyrus volume is reduced before onset of plaque formation in PDAPP mice: A magnetic resonance microscopy and stereologic analysis. Proc Natl Acad Sci USA 100:1381–1386.

Revsin Y, Rekers NV, Louwe MC, Saravia FE, De Nicola AF, de Kloet ER, Oitzl MS. 2009. Glucocorticoid receptor blockade normalizes hippocampal alterations and cognitive impairment in streptozotocin-induced type 1 diabetes mice. Neuropsychopharmacology 34:747–758.

Roberson ED, Scearce-Levie K, Palop JJ, Yan F, Cheng IH, Wu T, Gerstein H, Yu GQ, Mucke L. 2007. Reducing endogenous tau ameliorates amyloid beta-induced deficits in an Alzheimer's disease mouse model. Science 316:750–754.

Rodriguez JJ, Olabarria M, Chvatal A, Verkhratsky A. 2009. Astroglia in dementia and Alzheimer's disease. Cell Death Differ 16:378–385.

Schaeffer EL, Figueiro M, Gattaz WF. 2011. Insights into Alzheimer disease pathogenesis from studies in transgenic animal models. Clinics (Sao Paulo) 66 (Suppl 1):45–54.

Selkoe DJ. 2000. Toward a comprehensive theory for Alzheimer's disease. Hypothesis: Alzheimer's disease is caused by the cerebral accumulation and cytotoxicity of amyloid beta-protein. Ann NY Acad Sci 924:17–25.

Senitz D, Reichenbach A, Smith TG, Jr. 1995. Surface complexity of human neocortical astrocytic cells: changes with development, aging, and dementia. J Hirnforsch 36:531–537.

Simon AM, Schiapparelli L, Salazar-Colocho P, Cuadrado-Tejedor M, Escribano L, Lopez dM, Del Rio J, Perez-Mediavilla A, Frechilla D. 2009. Overexpression of wild-type human APP in mice causes cognitive deficits and pathological features unrelated to Abeta levels. Neurobiol Dis 33:369–378.

Spilman P, Podlutskaya N, Hart MJ, Debnath J, Gorostiza O, Bredesen D, Richardson A, Strong R, Galvan V. 2010. Inhibition of mTOR by rapamycin abolishes cognitive deficits and reduces amyloid-beta levels in a mouse model of Alzheimer's disease. PLoS One 5:e9979.

Steele ML, Robinson SR. 2012. Reactive astrocytes give neurons less support: Implications for Alzheimer's disease. Neurobiol Aging 33: 423–413.

Taglialatela G, Hogan D, Zhang WR, Dineley KT. 2009. Intermediate- and long-term recognition memory deficits in Tg2576 mice are reversed with acute calcineurin inhibition. Behav Brain Res 200:95–99.

van de Nes JA, Nafe R, Schlote W. 2008. Non-tau based neuronal degeneration in Alzheimer's disease—An immunocytochemical and quantitative study in the supragranular layers of the middle temporal neocortex. Brain Res 1213:152–165.

Verkhratsky A, Sofroniew MV, Messing A, Delanerolle NC, Rempe D, Rodriguez Arellano JJ, Nedergaard M. 2012. Neurological diseases as primary gliopathies: A reassessment of neurocentrism. ASN Neuro.

Vijayan VK, Geddes JW, Anderson KJ, Chang-Chui H, Ellis WG, Cotman CW. 1991. Astrocyte hypertrophy in the Alzheimer's disease hippocampal formation. Exp Neurol 112:72–78.

West MJ, Kawas CH, Martin LJ, Troncoso JC. 2000. The CA1 region of the human hippocampus is a hot spot in Alzheimer's disease. Ann NY Acad Sci 908:255–259.

Wilcock DM, Gordon MN, Morgan D. 2006. Quantification of cerebral amyloid angiopathy and parenchymal amyloid plaques with Congo red histochemical stain. Nat Protoc 1:1591–1595.

Wright AL, Zinn R, Hohensinn B, Konen LM, Beynon SB, Tan RP, Clark IA, Abdipranoto A, Vissel B. 2013. Neuroinflammation and neuronal loss precede abeta plaque deposition in the hAPP-J20 mouse model of Alzheimer's disease. PLoS One 8:e59586.